NANO LETTERS

Letter

pubs.acs.org/NanoLett

Adiabatically Tapered Hyperbolic Metamaterials for Dispersion Control of High-k Waves

Paul R. West,[†,§] Nathaniel Kinsey,[†,§] Marcello Ferrera,[†,‡] Alexander V. Kildishev,[†] Vladimir M. Shalaev,[†] and Alexandra Boltasseva*[,†]

[†]School of Electrical and Computer Engineering and Birck Nanotechnology Center, Purdue University, West Lafayette, Indiana United States

[‡]School of Engineering and Physical Sciences, Heriot-Watt University, David Brewster building, Edinburgh, Scotland EH14 4AS, United Kingdom

ABSTRACT: Hyperbolic metamaterials (HMMs) have shown great promise in the optical and quantum communities due to their extremely large, broadband photonic density of states. This feature is a direct consequence of supporting photonic modes with unbounded **k**-vectors. While these materials support such high-k waves, they are intrinsically confined inside the HMM and cannot propagate into the far-field, rendering them impractical for many applications. Here, we demonstrate how the magnitude of **k**-vectors can be engineered as the propagating radiation passes through media of differing dispersion relations (including type II HMMs and dielectrics) in the in-plane direction. The total outcoupling efficiency of waves in the in-plane direction is shown to be on average 2 orders of magnitude better than standard out-of-plane outcoupling methods. In addition, the outcoupling can be further enhanced using a proposed tapered HMM waveguide that is fabricated using a shadowed glancing angle deposition technique; thereby proving the feasibility of the proposed device. Applications for this technique include converting high-k waves to low-k waves that can be out-coupled into free-space and creating extremely high-k waves that are quickly quenched. Most importantly, this method of in-plane outcoupling acts as a bridge through which waves can cross between the regimes of low-k waves in classical dielectric materials and the high-k waves in HMMs with strongly reduced reflective losses.

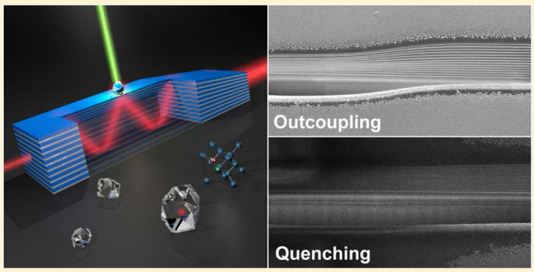

KEYWORDS: *Metamaterials, hyperbolic metamaterials, plasmonics, purcell, glancing angle deposition*

Hyperbolic metamaterials (HMMs) are a class of highly anisotropic metamaterials[1−3] whose namesake comes from their unique hyperbolic dispersion relation, associated with a genus of exotic properties.[4−6] In theory, the hyperbolic dispersion curve is unbounded, meaning these materials are able to support wavevectors that are extremely large in magnitude. Because the photonic density of states (PDOS) is proportional to the cube of the maximum allowed **k**-vector supported by the HMM ($\rho \approx k_{max}{}^3$),[7−9] HMMs have led to many unprecedented devices across a broad range of photonic applications.[9,10] By using a cylindrical HMM structure, an object with subwavelength features can be resolved in the far-field (known as a "hyperlens").[11,12] Furthermore, placing single-photon emitters in the vicinity of an HMM can provide a drastic Purcell enhancement over a broad spectral range and can therefore enhance the emitter's spontaneous emission rate.[13−19]

Because the individual elements (layers) of HMMs are much smaller than the wavelength of incident light, their effective, or bulk, material properties can be approximated by using the "effective medium theory" (EMT). By considering the optical properties of the constituent materials and their filling fraction, the effective response of the entire HMM structure can be approximated by eqs 1 and eq 2 with a dispersion curve given by eq 3.[20]

$$\varepsilon_{\parallel} = \varepsilon_m + (1 - f_m)\varepsilon_d \tag{1}$$

$$\varepsilon_{\perp}^{-1} = \frac{f_m}{\varepsilon_m} + \frac{(1 - f_m)}{\varepsilon_d} \tag{2}$$

$$\frac{k_x^2 + k_y^2}{\varepsilon_{\perp}} + \frac{k_z^2}{\varepsilon_{\parallel}} = \left(\frac{\omega}{c}\right)^2 \tag{3}$$

As can be seen from these equations, the material's electric response is strongly dependent on the metallic filling fraction (f_m), where two types of HMMs can be made. A "type I HMM" has a negative permittivity in the z-direction (along light propagation) and positive permittivity in the $x-y$ directions and can be realized, for example, with metallic rods in a dielectric host.[21] Likewise, a "type II HMM" can be realized by alternating layers of metal/dielectric thin films, producing a negative permittivity in the $x-y$ (in-plane) directions and a

Received: October 6, 2014
Revised: December 1, 2014

   dx.doi.org/10.1021/nl5038352 | *Nano Lett.* XXXX, XXX, XXX−XXX

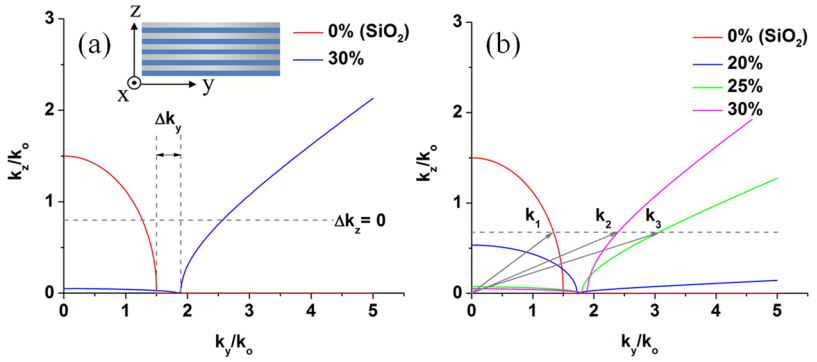

Figure 1. Dispersion relations for various dielectric and HMM structures: (a) Waves propagating in the z-direction cannot be coupled to air or SiO_2 due to a momentum mismatch while waves propagating in the in-plane direction can be coupled to SiO_2. Inset shows a schematic of the HMM with directions for reference. (b) Dispersion relation for various dielectric/HMMs as a function of metallic filling fraction.

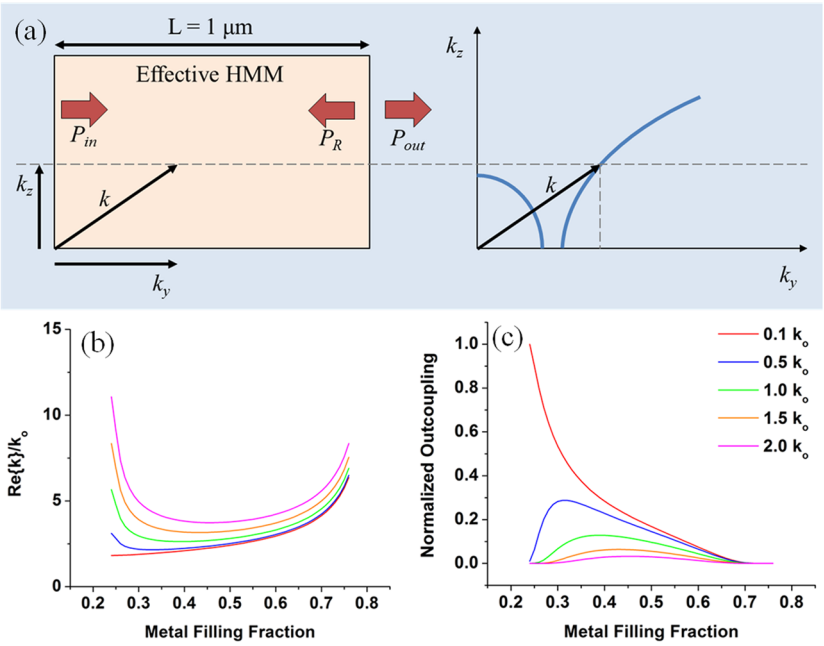

Figure 2. (a) Schematic of the effective medium model where a given magnitude of k_z is chosen and used to calculate the magnitude of the corresponding wavevector k. By considering the propagation losses in the y-direction (along the waveguide) and reflection losses at the HMM-air interface, the normalized outcoupled power is determined. We note that every wavevector is chosen to have the same input power. (b) Magnitude of real wavevector versus filling fraction for several k_z values. (c) Normalized power outcoupled for waves traveling in-plane for a 1 μm long silver-SiO_2 HMM versus the metal filling fraction for several magnitudes of k_z. Only filling fractions of 25−75% are considered since this is the range where the metamaterial is hyperbolic.

positive permittivity in the z-direction (perpendicular to the layers).[4] In this work, we primarily consider a type II HMM, although the discussion could be adapted and applied to a type I HMM as well.

While HMMs allow for very interesting physics due to their extreme anisotropy, the main challenge in taking full advantage of these materials is extracting (outcoupling) the supported high-k waves into free space. Purcell enhancements as high as 100× have been predicted for emitters near an HMM structure, and while one experiment has realized an enhancement of 80×,[13] other experiments have only reported enhancements less than a factor of 10.[14−16] Ideally, the large decrease in the decay rate of an emitter would be dominated by propagating modes (i.e., which can be directly collected by traditional optics) but for HMM structures the enhancement is mainly due to the coupling to high-k modes within the HMM.[17] As a result, the decrease in the lifetime does not correspond to a similar increase in the emission rate with only enhancements of ∼2× being observed for radiative modes.[14] However, if the high-k modes that are propagating within the HMM could be converted or coupled into low-k modes that exist within dielectrics, it may be possible to observe radiative enhancements which approach the large Purcell factors.

Traditionally, emission enhancement experiments are completed in the out-of plane (z-direction) for ease of confocal viewing and emitter excitation. However, in principle type II HMMs cannot couple to waves traveling in the out-of-plane direction due to momentum conservation. Previous works have observed emission in this direction as a result of surface imperfections (defects, scatterers, etc.) but these effects are generally not controllable and are inefficient. Gratings have been proposed as a means to enhance the outcoupling efficiency, either with a "bulls-eye" structure,[18] or more recently as an array of nanoholes.[19] While these techniques do increase

dx.doi.org/10.1021/nl5038352 | Nano Lett. XXXX, XXX, XXX−XXX

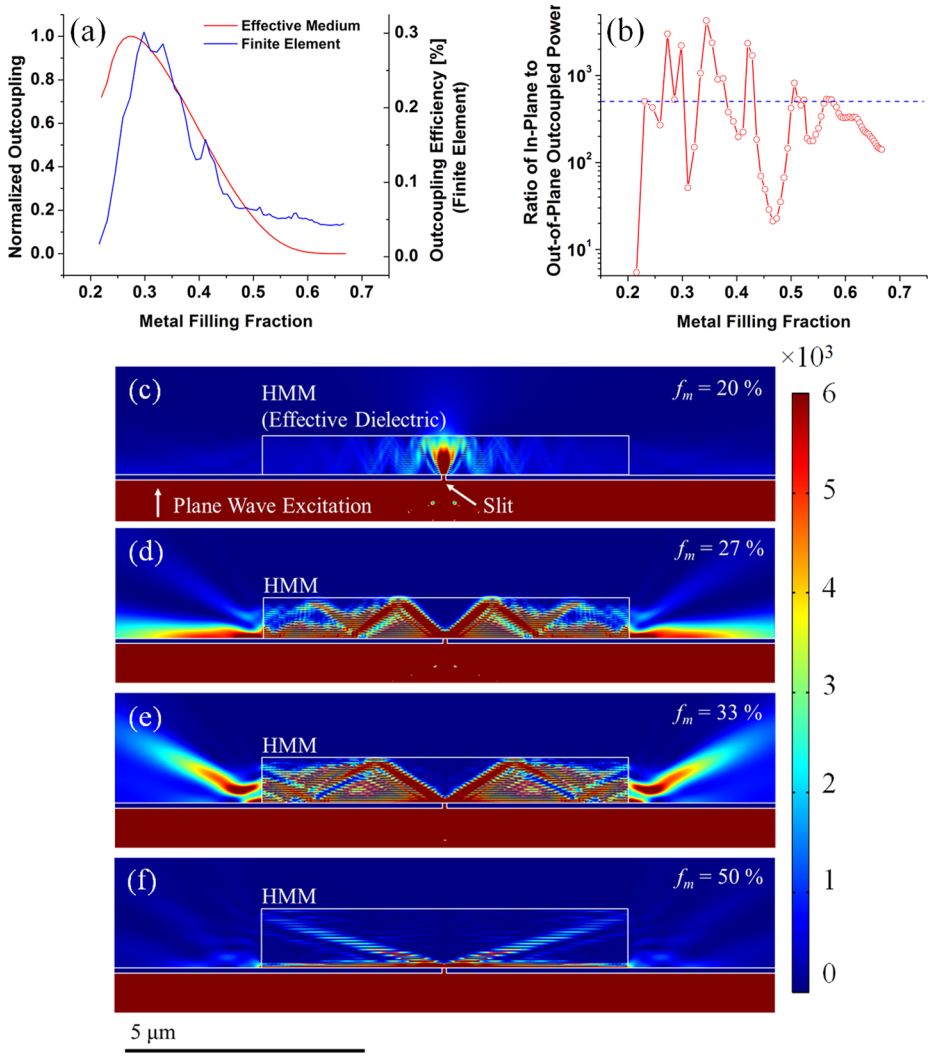

Figure 3. (a) Normalized incident power density outcoupled versus filling fraction for the effective medium approximation with wavevectors $0 < |k_z| < 10k_o$ and from the finite element numerical model using a 100 nm slit as the high-k scatterer. The efficiency of outcoupling is also shown on the righthand axis for the finite element simulation only (b) Ratio of the power outcoupled through the in-plane direction and the out-of-plane direction versus the HMM metal filling fraction. (c–f) Power distribution normalized to the input power for varying filling fractions, illustrating the maximal outcoupling. (c) Twenty percent filling fraction (Ag 10 nm, SiO_2 40 nm). (d) Twenty-seven percent filling fraction (Ag 15 nm, SiO_2 40 nm). (e) Thirty-three percent filling fraction (Ag 20 nm, SiO_2 40 nm). (f) Fifty percent filling fraction (Ag 40 nm, SiO_2 40 nm). Note that the oscillations in the numerical simulation (as seen in a and b) result from interference of several emission points.

the outcoupling efficiency leading to a reported emission enhancement of 18×) they are inherently narrow-band, and do not take full advantage of the broadband nature of HMMs. To mitigate some of the short-comings of HMMs, we look toward the natural ability of type II HMMs to outcouple high-k waves along the in-plane (x–y) direction and propose a new tapered HMM waveguide structure to allow for the engineering of outcoupling properties.

In-Plane Coupling of High-k Waves for Type II HMMs. The first point of our study is to investigate the potential for outcoupling light from HMM structures. Our HMM consists of silver as the metal and SiO_2 as the dielectric material. Operating at a wavelength of 476 nm, these materials have permittivities of $\varepsilon_m = -8.26 + 0.2i$ (silver), and $\varepsilon_d = 2.25$ (SiO_2).[22] Figure 1b shows the dispersion relation for HMMs of different metallic filling fractions, ranging from 0% (pure dielectric) to 30%, where the material clearly exhibits hyperbolic dispersion at the wavelength of interest.

Figure 1a is the dispersion curve showing the allowed **k**-vectors that are able to propagate in SiO_2, and a type II Ag/SiO_2 HMM. It is important to note that for a wave incident on a material in the z-direction, the in-plane (x- and y-components) of the field must be conserved. As a result of the HMM dispersion, light cannot be directly coupled between the HMM and dielectric due to the abrupt jump in k_y. Therefore, the waves at an HMM/dielectric interface will experience total reflection (because this interface is ideal and does not incorporate roughness or defects). However, the situation is different for waves traveling in the y-direction along the HMM layers where the k_z component of the field must be conserved. In this case, the **k**-vector can pass between dispersion curves in a horizontal manner with some reflective losses, as shown in Figure 1b. From this figure, it can be seen that wave vectors can transform from k_3 to k_2 as the metal filling fraction changes between 25% and 30% and from k_2 to k_1 as the wave passes from the HMM with 30% filling fraction into SiO_2 (along the gray line in Figure 1b). In this way, the type II

dx.doi.org/10.1021/nl5038352 | Nano Lett. XXXX, XXX, XXX–XXX

HMM is capable of outcoupling to free-space in the in-plane direction, and by optimizing the filling fraction of the HMM the efficiency can be maximized. For example, for a given value of k_z the metal filling fraction of 30% (k_2) allows a wave with a lower magnitude of momentum than a medium with a filling fraction of 25% (k_3).

To further investigate this phenomenon, the outcoupling versus filling fraction, including both reflective and propagation losses, of a 1 μm long HMM (i.e., HMM is 1 μm long in the y-direction) was determined for several different magnitudes of k_z, see Figure 2a. While the reflection losses are monotonically increasing as the filling fraction increases (i.e., $n_{\|}$ increases with increasing filling fraction), the propagation losses have a minimum for a certain wavevector, leading to a maximized output for a specific filling fraction (for a given magnitude of k_z, see Figure 2b,c). This can be intuitively understood by considering the HMM dispersion diagram. For wavevectors with a large k_z component and a small filling fraction, the magnitude of the resulting wavevector is very large. As the filling fraction increases, the hyperbola opens such that a wavevector with a given k_z has a smaller magnitude and correspondingly smaller propagation losses (i.e., k_3 to k_2 in Figure 1b). However, for large filling fractions where the HMM is nearly metallic, all modes propagating in the bulk begin experiencing significant attenuation as only surface waves are allowed in the nearly effective metal. As a result, there is an optimal outcoupling condition. We also note that for larger wavevectors, the optimal outcoupling position is at higher metal filling fractions although the overall efficiency decreases.

To test the validity of the EMT model for outcoupling, a simulation of the planar HMM structure with varying filling fraction was completed using the Finite Element Method (FEM). In this structure, 15 pairs of metal-dielectric layers were used to form the HMM with a length of 5 μm. A small subwavelength-sized slit was cut into a lossy metallic layer to scatter high-k waves into the HMM from a plane wave source. The percentage of the incident power outcoupled both in-plane and out-of-plane by the structure was measured as a function of the filling fraction for a slit width of 100 nm. However, because this metallic slit does not discriminate which wavevectors are launched into the HMM there will be more than just a single mode propagating within the structure. As such, the out-coupling efficiencies for wavevectors with $0 < |k_z| < 10k_o$ are summed in the EMT calculation, assuming equal power in all modes. Wavevectors with k_z larger than $10k_o$ are not considered as they experience significant propagation losses and are a small correction to the final output. The graphs of the normalized in-plane outcoupling from the EMT calculation and from the FEM simulation are shown in Figure 3a with selected power distributions normalized to the input power in Figure 3c–f. We also plot the absolute outcoupling efficiency of the FEM simulation as a secondary axis in Figure 3a. For comparison of the outcoupling efficiencies, the input power was measured 1 μm below from the input slit as the difference between the radiated and reflected power (effectively measuring the power coupled into the HMM), the power coupled in the traditional out-of-plane direction was measured 1 μm above the structure for the length of the HMM, and the power outcoupled in the in-plane direction was measured 1 μm to the right of the structure for the height of the simulation space. Please note that the simulation was completed for a half-space to the right of the lateral symmetry line of the structure. All figures are plotted as a mirror image for clarity although all power measurements were completed only on the half-space.

In general there is an overall good agreement between the shapes of the "outcoupling versus filling fraction" curves reported in Figure 3a predicting the maximal outcoupling efficiency near a filling fraction of 30% for this particular HMM design. It is important to note that a relatively simple estimation of the efficiency assuming all scattered modes contain equal power coupled with an EMT approximation proves to be a good starting point for analysis and optimization. This method captures the main essence of the distribution as well as the optimal filling fraction for outcoupling, achieving a good agreement with the more complex full-wave simulations. The slight shift in the peak (~4% in filling fraction) can be justified by the nonuniform distribution of the slit when scattering high-k waves (i.e., one wavevector contains more power than another). In addition, this error is within typical fabrication tolerances, corresponding to a 3 nm change in thickness of the metal layer for an HMM with a 20 nm silver layer and a 40 nm silica layer. However, if we compare the ratio of the power outcoupled in the in-plane direction with the power outcoupled in the out-of-plane direction, we find that on average the in-plane approach achieves ~500× more power than the out-of-plane direction with a peak of more than 3000× as shown in Figure 3b. The beating pattern noted in the outcoupled power is due to interference between multiple outcoupling centers. These can be seen in Figure 3c–f where surface waves on the top and bottom of the HMM interfere with the volume plasmon emission. This could be reduced by integrating the power closer to the HMM structure, however we wanted to ensure that the light was coupling into the far-field so the power was measured 1 μm away from the HMM facet.

To further illustrate the potential of outcoupling from an HMM structure in-plane, fabricated samples were tested experimentally using gratings cut into the HMM by focused ion beam milling that serves as high-k scatterers. These HMMs consisted of 15 pairs of SiO_2 and silver layers with a thin (~1 nm) wetting layer of germanium in between. The silver thickness was 20 nm and the SiO_2 thickness was 58 nm, resulting in a filling fraction of ~26%. The edge of the sample was also milled flat to a length of 5 μm (as measured from the edge of the gratings) to allow for viewing of the outcoupled energy. The outcoupled energy was collected by a Scienscope CCD camera connected to an objective system with adjustable magnification between 5–120×. The sample was tested and designed to operate at a wavelength of 476 nm (NKT Photonics SuperK!). In Figure 4a, the structure and excitation light coupled to the gratings are shown from the top where the outcoupled light is viewed from the left. The light collected by the output objective is shown in Figure 4b. The large bright spot is light directly scattered from the gratings into the camera, but a smaller second mode is present just below (circled) that corresponds to the output facet of the HMM structure. Despite a low contrast between the two signals, the observed mode is only able to be captured when the viewing system is focused on the output facet of the structure. Altering the focal length of the system slightly results in a disappearance of this mode. Traditionally, out-of-plane experiments require very sensitive detectors or photon counters to observe the outcoupled energy. However, with an in-plane approach the outcoupled energy is strong enough to be captured by a standard CMOS CCD camera.

dx.doi.org/10.1021/nl5038352 | Nano Lett. XXXX, XXX, XXX–XXX

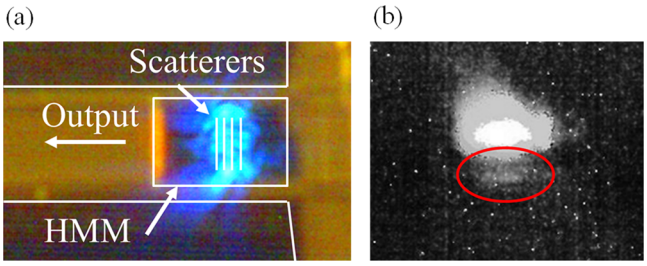

Figure 4. (a) Top view of the illuminated HMM structure. The light is being scattered by the grating couplers. The modal output was observed from the left. (b) Modal output of the HMM waveguide structure demonstrating the ability to outcouple high-k waves scattered inside the HMM to free space with an in-plane approach.

Adiabatically Tapered HMM. To outcouple light from an HMM a minimal wave vector mismatch is desirable to reduce both the propagation and reflective losses. However, the optimal outcoupling filling fraction is generally different than the optimal filling fraction for a high PDOS and spontaneous emission enhancement. For example, the PDOS is proportional to $1/a^3$ (or $k_{max}{}^3$) where a is the distance between the centers of the two adjacent layers.[7−9] Therefore, for spontaneous emission enhancement, it is desirable to have the layers as thin as possible. Unfortunately, there are fabrication challenges in growing metal films thinner than approximately 5−10 nm, so the thickness of the dielectric would be made as thin as possible while still maintaining hyperbolic dispersion. However, high filling fractions (say ∼50%) incur significant propagation losses and are not optimal for outcoupling. Therefore, the filling fraction should be lowered to provide optimal outcoupling. To decouple the optimization of both HMMs, we propose a smooth in-plane tapering of the metal filling fraction. Because of this adiabatic transition, high-k waves can couple between these HMMs with minimal reflective loss, as the tapering provides a continual impedance-matched transition.

The length of the tapered transition should be larger than the operating wavelength to avoid abrupt transitions (large reflections), while not being too long as material losses in the constituent metal will decrease the device's internal efficiency. Additionally, the number of metal−dielectric layers in the structure should be greater than five so that the structure behaves as an HMM. However, the number of layers can be increased depending on the desired size of the outcoupling end of the waveguide. The emitter should be placed on top of or inside the HMM optimized for PDOS enhancement, and as close as possible to the tapered region. The enhanced emission will travel into this HMM, through the adiabatically tapered waveguide, and be outcoupled into air (or other dielectric medium) with maximized outcoupling efficiency. An example of the structure is depicted in Figure 5a.

While a tapered waveguide can be designed to optimize the outcoupling of high-k waves into free-space, these structures can also be used to quench the high-k modes traversing through a tapered waveguide. An example of the structure is depicted in Figure 5b. By using the waveguide in a reverse manner and decreasing the metal filling fraction past the HMM-dielectric transition, high-k waves inside an HMM continually increase in magnitude (see Figure 2b), resulting in slower propagation speed and increased loss. This technique has been investigated previously for metal-insulator-metal plasmonic waveguides as a means of quenching[23] and also as a method for drastically increasing the energy density for nonlinear applications.[24−27] Another recent work has also considered tapered HMMs as a method for absorption, although they are tapered in the in the z-direction (perpendicular to the layers) and not along the layers as we have shown here and the absorption relies on resonant absorption in the structure instead of control of the material wavevector.[28]

Numerical Simulations of the Device. To simulate the HMM with a tapered structure, a commercial FEM software package (COMSOL Multiphysics) was used. Each structure has 15 layers of silver and 16 of SiO_2 (one extra on the top). The simulated structure consists of three parts, a flat (nontapered) HMM with metallic gratings for scattering high-k waves into the structure, a tapered HMM section to the left of the incoupling structure, and a nontapered HMM to the right of the incoupling structure for comparison (see Figure 6). This design is representative of the final fabricated structure and allows for a direct evaluation of the tapered structure by comparing its output to the nontapered side of the same device. One of the waveguides has a filling fraction that tapers to zero for quenching, while the other two waveguides have a filling fraction which are tapered to optimize outcoupling. Two subwavelength scattering slits were cut into a chrome mask to create high-k waves inside the HMM. These slits are 100 nm wide, separated by 200 nm, and are placed an equal distance from the ends of the structure. Both the tapered and flat waveguides are set to a length of 5 μm. We also note that due to the varying filling fraction (impedance) of the incoupling HMM, the power inside the HMM varies for each structure. As

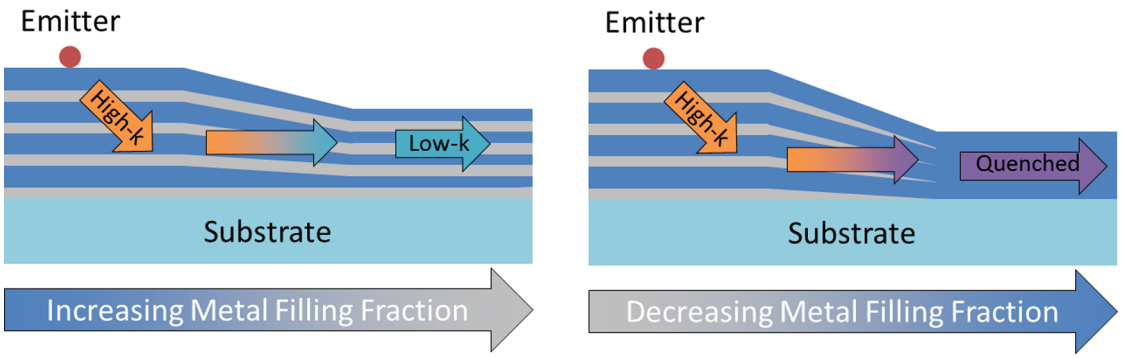

Figure 5. Illustrations of two possible adiabatically tapered type II HMM structures for (a) outcoupling of enhance emission of single-photon emitters and (b) quenching of high-k waves passing through the metamaterial with decreasing metallic filling fraction.

dx.doi.org/10.1021/nl5038352 | Nano Lett. XXXX, XXX, XXX−XXX

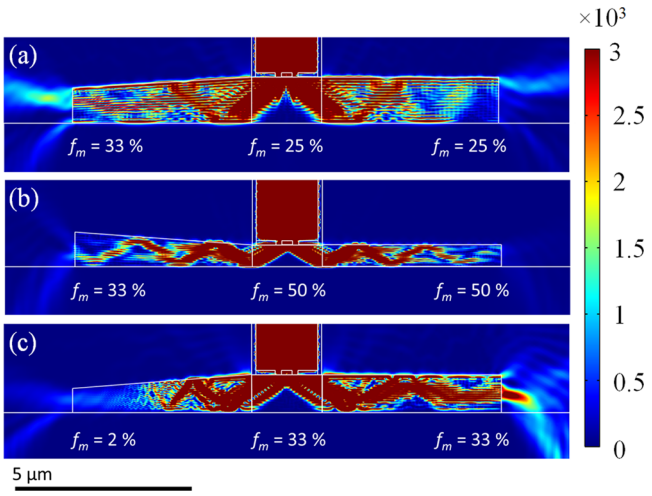

Figure 6. Normalized time average power flow of high-k waves propagating through dual-ended structures where one end is tapered and the other remains flat. The outcoupling structure (a) tapers the SiO_2 thickness from 60 to 40 nm while the silver remains constant at 20 nm. The outcoupling structure (b) tapers the SiO_2 thickness from 20 to 40 nm while silver remains constant at 20 nm. The quenching structure in (c) tapers the silver thickness from 20 to 2 nm while keeping the SiO_2 thickness constant at 40 nm.

a result we present simulation results that are normalized to the input power as measured 1 μm above the slit.

The design shown in Figure 5a demonstrates the possibility of tapering to convert the high-k waves inside the HMM into waves with a lower momentum which can outcouple more efficiently into air. This structure was numerically simulated for two different initial filling fractions of 25 and 50%. For the structure with a 25% initial filling fraction, the silver thickness is constant at 20 nm and the SiO_2 thickness is tapered from 60 to 40 nm, reaching the optimal outcoupling point of ~33%. Consequently, the intensity observed at the tapered end of the waveguide, shown in Figure 6a, is 164% greater than the nontapered HMM. For the structure with a 50% initial filling fraction, the silver thickness remains constant at 20 nm and the SiO_2 thickness is tapered from 20 to 40 nm. In this case, 247% more power was outcoupled from the tapered waveguide, Figure 6b, when compared to the nontapered waveguide. It is also important to note that the efficiency of this device is not fully optimized and could be improved based on the magnitude of the **k**-vector of interest, the length of the waveguide, and the metal/dielectric materials used to create the HMM.

Alternatively, the quenching structure, based on the design in Figure 5b, tapers the silver thickness from 20 to 2 nm while the SiO_2 thickness remains constant at 40 nm. The result of numerical simulation for this structure is shown in Figure 6c. Clearly, the modes propagating along the tapered region encounter significant propagation loss as the magnitude of **k** increases with the decreasing metal filling fraction. The power outcoupled from the tapered structure is 5× less than the power outcoupled from the nontapered portion of the waveguide. Thus, the device in Figure 6c is a possible solution for efficient light absorption (i.e., in-line waveguide termination without reflection). Additionally, such a system could be realized in hyperbolic metasurfaces to enable broadband perfect absorbers.[25]

As a final verification of the tapered structure, an electric point dipole is placed inside the HMM to observe the outcoupling potential. To obtain the maximum effect of the HMM and achieve the largest Purcell enhancement, the emitter should be placed inside the HMM. In Figure 7, we present a

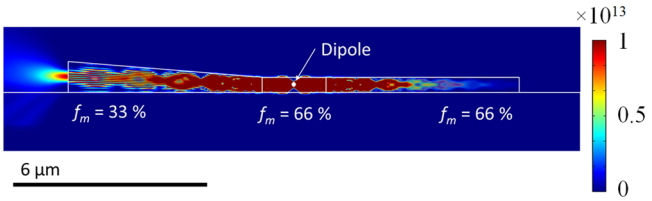

Figure 7. Power distribution for an electric dipole placed inside an HMM with high filling fraction for maximal PDOS, and tapered to increase the outcoupling efficiency. The structure is tapered from a filling fraction of 66% (silver thickness of 20 nm and SiO_2 thickness of 10 nm) to a filling fraction of 33% (silver thickness of 20 nm and a SiO_2 thickness of 40 nm).

tapered HMM waveguide structure with a 6 μm tapering/flat length where the initial filling fraction is 66%, corresponding to a silver thickness of 20 nm and a SiO_2 thickness of 10 nm (to form unit cell of 30 nm). This extremely small unit cell achieves a large PDOS (proportional to $1/a^3$) to maximize the effect of the Purcell enhancement. However, as can be seen in the figure, the high filling fraction results in a large propagation loss which negates any effect that the high Purcell enhancement would have provided. By tapering the waveguide to a lower filling fraction, in this case to 33% (20 nm silver and 40 nm silica), a significant portion of the energy can be outcoupled to the far-field. In fact, the tapered waveguide achieves 153× more power outcoupled than the nontapered HMM for the same length. If we consider the enhancement of outcoupling for in-plane versus out-of-plane, the power outcoupled in-plane is 1614× more than is extracted vertically. The power outcoupled in-plane was measured 1 μm from the ends of the structure and the power outcoupled out-of-plane was measured 1 μm above the structure for the length of the HMM.

Fabrication. In practice, these proposed adiabatically tapered type II HMM structures can be fabricated in two ways: by increasing the thickness of the metallic layers or by decreasing the thickness of the dielectric layers. The tapered HMM structures were fabricated using a new shadowed deposition technique in addition to glancing angle deposition.[29,30] This technique is briefly summarized in Figure 8. By depositing a material at a steep angle over the edge of a

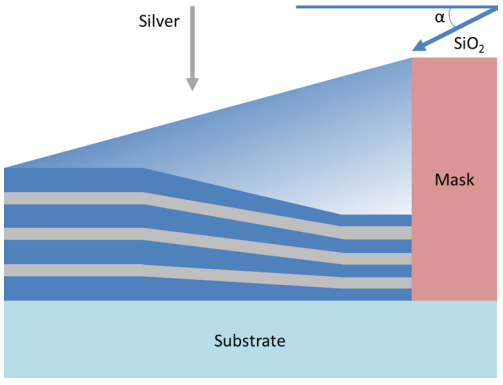

Figure 8. Schematic of the fabrication method for the tapered HMM structure using a shadowed glancing angle deposition technique in combination with traditional normal incidence deposition.

dx.doi.org/10.1021/nl5038352 | *Nano Lett.* XXXX, XXX, XXX–XXX

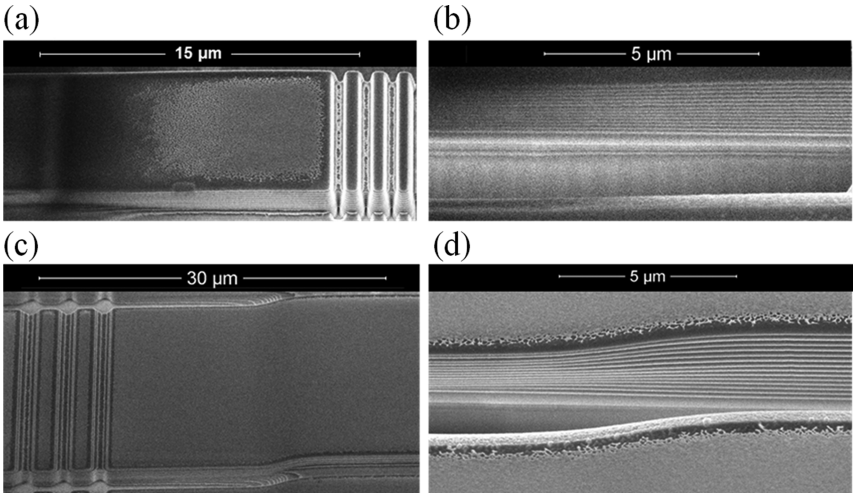

Figure 9. (a) Quenching sample made using glancing angle deposition where the metal filling fraction is tapered from 26% to 0% from right to left. (b) Enlarged view of the tapered portion of the quenching waveguide. (c) Outcoupling sample where the filling fraction is tapered from 26% to 35% from right to left. (d) Enlarged view of the tapered portion of the outcoupling waveguide. The reported SEM images were obtained after implementing focused ion beam cuts on the multilayer structure.

predefined mask, a gradient in the deposition material is formed due to particle diffraction. The gradient results in a variation of thickness of the deposited material with distance. By alternating the deposition of two materials between a vertical and a glancing angle, a layer of uniform thickness (vertical deposition) and a layer of tapered thickness (angled deposition) can be formed. This allows the filling fraction of the HMM to be smoothly transitioned between two desired values. The slope of the taper can be controlled by adjusting the angle of shadowed deposition (shown as α in Figure 8). An angle near normal will result in an abrupt taper and a shallow angle will result in a longer taper. An example fabrication of the HMM with increasing filling fraction is shown in Figure 8 where the fraction of SiO_2 is reduced while the silver thickness is maintained constant.

Two samples were fabricated using this technique, one with an increasing filling fraction (outcoupling) and one with a decreasing filling fraction (quenching). The outcoupling sample was fabricated using a glancing angle deposition system (PVD Systems) with SiO_2 deposition at an angle of 20° over a 60 μm tall mask and the silver was deposited normally. This structure tapers the SiO_2 from 58 to 37 nm while the silver remains constant at 20 nm, a filling fraction of 26 to 35%. For the quenching sample, silver was deposited at a 20° over a 60 μm tall mask and SiO_2 was deposited at a normal incidence. A thin wetting layer of germanium (~1 nm) was also deposited before each silver film to enable continuous growth below 7 nm in thickness.[31,32] In this sample, the silver was tapered from 20 nm down to 0 nm and the SiO_2 thickness remained constant at 58 nm, a filling fraction of 26 to 0%. The deposition process was repeated 15 times to ensure bulk HMM behavior. Images of the final fabricated samples are shown in Figure 9. To enable the light to couple into the HMM, a series of subwavelength slits were milled into the structures using a focused ion beam, acting to scatter light into high-k modes within the HMM. In our experiments, a focused laser beam was incident on the milled slits to excite high-k modes within the HMMs. A measurable output signal from the HMM structures was detected in the far field, however, the accurate measurement of emission from the HMMs requires a more dedicated setup that allows for complete elimination of the incident radiation at the detection point. Additional testing of the fabricated HMM structures is ongoing.

Conclusions. While HMMs provide a medium with extraordinary fundamental optical properties (including extremely high broadband PDOS), these metamaterials have remained elusive for use in practical devices because their extraordinary optical properties are difficult to observe in the far-field. Here, we propose a design for outcoupling broadband high-k waves from an HMM with relatively high efficiencies. Rather than outcoupling in the out-of-plane direction, here we study the more efficient in-plane approach which achieves 500× more power outcoupled on average. Furthermore, we provide a design for a waveguide structure with in-plane tapered metal filling fraction through which high-k waves can be efficiently coupled to free-space, or quenched. We have also applied an advanced fabrication technique based on glancing angle deposition to demonstrate that realization of the reported tapered and nontapered HMMs with on-demand metal filling fractions is practical.

The proposed strategy allows for a simultaneously optimized enhancement in PDOS and optimized outcoupling of the high-k waves into free-space. Most importantly, this work bridges the gap between the high-k waves of HMMs and low-k waves of dielectrics, joining the classical field of dielectric optics with the modern field of hyperbolic metamaterials.

AUTHOR INFORMATION

Corresponding Author

*E-mail: aeb@purdue.edu.

Author Contributions

[§]P.R.W. and N.K. contributed equally to this work.

The manuscript was written through contributions from all authors. P.R.W.'s contributions were through fabrication and numerical simulation. N.K.'s contributions were through theoretical calculation, numerical simulation, experimentation, and project conceptualization. M.F.'s contributions were through experimentation and project conceptualization. A.V.K., V.M.S., and A.B. supervised and guided the work. All authors have given approval to the final version of the manuscript.

Funding

We would like to acknowledge ARO Grant 56154-PH-MUR, and AFOSR Grant FA9550−12−1−0024

Notes

The authors declare no competing financial interest.

■ ABBREVIATIONS

HMM hyperbolic metamaterial; PDOS photonic density of states

■ REFERENCES

(1) Zheludev, N. I.; Kivshar, Y. S. From metamaterials to metadevices. *Nat. Mater.* **2012**, *11*, 917−924.
(2) Liu, Y.; Zhang, X. Metamaterials: a new frontier of science and technology. *Chem. Soc. Rev.* **2011**, *40*, 2494−2507.
(3) Simovski, C. R. Material Parameters of Metamaterials (a Review). *Opt. Spectrosc.* **2009**, *107*, 726−753.
(4) Poddubny, A.; Iorsh, I.; Belov, P.; Kivshar, Y. Hyperbolic metamaterials. *Nat. Photonics* **2013**, *7*, 948−957.
(5) Noginov, M. A.; Laping, M.; Podolskiy, V. A.; Kivshar, Y. Focus issue: hyperbolic metamaterials. *Opt. Express* **2013**, *21*, 14895.
(6) Drachev, V. P.; Podolskiy, V. A.; Kildishev, A. V. Hyperbolic metamaterials: new physics behind a classical problem. *Opt. Express* **2013**, *21*, 15048−15064.
(7) Jacob, Z.; Kim, J.-Y.; Naik, G. V.; Boltasseva, A.; Narimanaov, E. E.; Shalaev, V. M. Engineering Photonic Density of States using Metamaterials. *Appl. Phys. B: Laser Opt.* **2010**, *100*, 215−218.
(8) Krishnamoorthy, H. N. S.; Jacob, Z.; Narimanov, E. E.; Kretzschmar, I.; Menon, V. M. Topological Transitions in Metamaterials. *Science* **2012**, *336*, 205−209.
(9) Jacob, Z.; Smolyaninov, I. I.; Narimanov, E. E. Broadband Purcell effect: Radiative decay engineering with metamaterials. *Appl. Phys. Lett.* **2012**, *100*, 181105.
(10) Tumkur, T. U.; Kitur, J. K.; Chu, B.; Gu, L.; Podolskiy, V. A.; Narimanov, E. E.; Noginov, M. A. Control of reflectance and transmittance in scattering and curvilinear hyperbolic metamaterials. *Appl. Phys. Lett.* **2012**, *101*, 091105.
(11) Jacob, Z.; Alekseyev, L. V.; Narimanov, E. E. Optical Hyperlens: Far-field imaging beyond the diffraction limit. *Opt. Express* **2006**, *14*, 8247−8256.
(12) Liu, Z.; Lee, H.; Xiong, Y.; Sun, C.; Zhang, X. Far-field optical hyperlens magnifying sub-diffraction-limited objects. *Science* **2007**, *215*, 1686−1686.
(13) Lu, D.; Kan, J. J.; Fullerton, E. E.; Liu, Z. Enhancing spontaneous emission rates of molecules using nanopatterned multilayer hyperbolic metamaterials. *Nat. Nanotechnol.* **2014**, *9*, 48−53.
(14) Shalaginov, M. Y.; Ishii, S.; Liu, J.; Irudayaraj, J.; Lagutchev, A.; Kildishev, A. V.; Shalaev, V. M. Broadband Enhancement of Spontaneous Emission from Nitrogen-Vacancy Centers in Nanodiamonds by Hyperbolic Metamaterials. *Appl. Phys. Lett.* **2013**, *102*, 173114.
(15) Kim, J.; Drachev, V. P.; Jacob, Z.; Naik, G. V.; Boltasseva, A.; Narimanov, E. E.; Shalaev, V. M. Improving the radiative decay rate for dye molecules with hyperbolic metamaterials. *Opt. Express* **2012**, *20*, 8100−8116.
(16) Noginov, M. A.; Li, H.; Barnakov, Y. A.; Dryden, D.; Nataraj, G.; Zhu, G.; Bonner, C. E.; Mayy, M.; Jacob, Z.; Narimanov, E. E. Controlling spontaneous emission with metamaterials. *Opt. Lett.* **2010**, *35*, 1863.
(17) Shalaginov, M. Y.; Vorobyov, V. V.; Liu, J.; Ferrera, M.; Akimov, A. V.; Lagutchev, A.; Smolyaninov, A. N.; Klimov, V. V.; Irudayaraj, J.; Kildishev, A. V.; Boltasseva, A.; Shalaev, V. M. Enhancement of single-photon emission from nitrogen-vacancy centers with TiN/(Al,Sc)N hyperbolic metamaterial. *Laser Photon. Rev.* **2014**, DOI: 10.1002/lpor201400185.
(18) Newman, W.; Cortes, C. L.; Jacob, Z. Enhanced and Directional single-Photon Emission in Hyperbolic Metamaterials. *J. Opt. Soc. Am. B* **2013**, *30*, 766−775.
(19) Sreekanth, K. V.; Krishna, K. H.; De Luca, A.; Strangi, G. Large spontaneous emission rate enhancement in grating coupled hyperbolic metamaterials. *Sci. Rep.* **2014**, *4*, 6340.
(20) Kidwai, O.; Zhukovsky, S. V.; Sipe, J. E. Effective-medium approach to planar multilayer hyperbolic metamaterials: Strengths and limitations. *Phys. Rev. A* **2012**, *85*, 053842.
(21) Prokes, S. M.; Glembocki, O. J.; Livenere, J. E.; Tumkur, T. U.; Kitur, J. K.; Zhu, G.; Wells, B.; Podolskiy, V. A.; Noginov, M. A. Hyperbolic and plasmonic properties of Silica/Ag aligned nanowire arrays. *Opt. Express* **2013**, *21*, 14962−14974.
(22) Ni, X.; Liu, Z.; Kildishev, A. V. PhotonicsDB: Optical Constants, https://nanohub.org/resources/PhotonicsDB, 2014.
(23) Stockman, M. I. Nanofocusing of optical energy in tapered plasmonic waveguides. *Phys. Rev. Lett.* **2004**, *93*, 137404.
(24) Verhagen, E.; Kuipers, L.; Polman, A. Enhanced Nonlinear Optical Effects with a Tapered Plasmonic Waveguide. *Nano Lett.* **2007**, *7*, 334−337.
(25) Verhagen, E.; Polman, A.; Kuipers, L. Nanofocusing in laterally tapered plasmonic waveguides. *Opt. Express* **2008**, *16*, 45−57.
(26) Davoyan, A. R.; Shadrivov, I. V.; Zharov, A. A.; Gramotnev, D. K.; Kivshar, Y. S. Nonlinear nanofocusing in tapered plasmonic waveguides. *Phys. Rev. Lett.* **2010**, *105*, 116804.
(27) Pile, D. F. P.; Gramotnev, D. K. Adiabatic and nonadiabatic nanofocusing of plasmons by tapered gape plasmon waveguides. *Appl. Phys. Lett.* **2006**, *89*, 041111.
(28) Ji, D.; Song, H.; Zeng, X.; Hu, H.; Liu, K.; Zhang, N.; Gan, Q. Broadband absorption engineering of hyperbolic metafilm patterns. *Sci. Rep.* **2014**, 4.
(29) Robbie, K.; Brett, M. J. Sculptured thin films and glancing angle deposition: Growth mechanics and applications. *J. Vac. Sci. Technol., A* **1997**, *15*, 1460.
(30) Robbie, K.; Sit, J. C.; Brett, M. J. Advanced techniques for glancing angle deposition. *J. Vac. Sci. Technol., B* **1998**, *16*, 1115.
(31) Chen, W.; Chen, K. P.; Thoreson, M. D.; Kildishev, A. V.; Shalaev, V. M. Ultrathin, ultrasmooth, and low-loss silver films via wetting and annealing. *Appl. Phys. Lett.* **2010**, *97*, 211107.
(32) Chen, W.; Thoreson, M. D.; Ishii, S.; Kildishev, A. V.; Shalaev, V. M. Ultra-thin ultra-smooth and low-loss silver films on a germanium wetting layer. *Opt. Express* **2010**, *18*, 5124−5134.